

Correlation holes and slow dynamics induced by fractional statistics in gapped quantum spin liquids

Oliver Hart,¹ Yuan Wan,^{2,3} and Claudio Castelnovo^{1,*}

¹*T.C.M. Group, Cavendish Laboratory, JJ Thomson Avenue, Cambridge CB3 0HE, United Kingdom*

²*Institute of Physics, Chinese Academy of Sciences, Beijing 100190, China*

³*Songshan Lake Materials Laboratory, Dongguan, Guangdong 523808, China*

(Dated: November 2019)

Abstract. Realistic model Hamiltonians for quantum spin liquids frequently exhibit a large separation of energy scales between their elementary excitations. At intermediate, experimentally relevant temperatures, some excitations are sparse and hop coherently, whereas others are thermally incoherent and dense. Here we study the interplay of two such species of quasiparticle, dubbed spinons and visons, which are subject to nontrivial mutual statistics – one of the hallmarks of quantum spin liquid behaviour. Our results for \mathbb{Z}_2 quantum spin liquids show an intriguing feedback mechanism, akin to the Nagaoka effect, whereby spinons become localised on temperature-dependent patches of expelled visons. This phenomenon has important consequences for the thermodynamic and transport properties of the system, as well as for its response to quenches in temperature. We argue that these effects can be measured in experiments and may provide viable avenues for obtaining signatures of quantum spin liquid behaviour.

Introduction

Topologically ordered phases of matter have attracted much attention over the past few decades [1, 2] thanks to their unusual behaviour, which is of fundamental interest and has potential applications in quantum information storage and processing [1, 3, 4]. Such states are characterised for example by subleading corrections to the ground state entanglement entropy [5, 6], and by a ground state degeneracy that depends on the genus of the space on which the system resides [7]. Their low-energy excitations often take the form of pointlike, fractionalised quasiparticles with anyonic statistics [8].

While concrete and unambiguous experimental evidence for these unusual ground state properties remains in general unavailable, the exchange statistics of the quasiparticles and their fractional quantum numbers offer some of the most promising routes to unique and experimentally accessible signatures of topological order [9, 10]. Examples of such excitations include the Laughlin quasiparticles of the fractional quantum Hall effect [11] or the Majorana fermions in Kitaev-like materials [12].

In the context of quantum spin liquids (QSLs)—topologically ordered phases that arise in frustrated magnets at low temperatures [13–15]—we reflect on the fact that realistic model Hamiltonians exhibiting QSL behaviour can often be constructed with [16, 17]: (i) a large, classical constraint that projects the Hilbert space onto an extensive set of local tensor product states; and (ii) quantum fluctuations. The fluctuations induce coherent superpositions of the tensor product states, endowing the system with quantum topological properties, but must not be strong enough to drive the system across a confinement/Higgs transition. In such systems, there are quasiparticles (that we dub spinons) that violate the classical constraint; these have a large energy cost Δ_s and smaller but significant hopping matrix elements of magnitude $t_s < \Delta_s$ (typically of the order of the quantum fluctuation—e.g., exchange—terms present in the system). There are also gapped excitations, which we

dub visons, that disturb the quantum phase coherence amongst the constrained states, whose energy cost Δ_v is perturbative in t_s/Δ_s in the deconfined phase and thence much smaller than both Δ_s and t_s . Typically, the characteristic magnitude of their hopping matrix elements is smaller still, $t_v < \Delta_v$. A case in point is indeed quantum spin ice [14] with small transverse terms. While this may not be considered an example of topological quantum order per se, its microscopic Hamiltonian is nonetheless an example of how one could realise a quantum spin liquid in experiment. It features a large projective energy scale and small transverse kinetic terms, which give rise to an eminently accessible temperature range where the results in our paper apply.

In this scenario, it is of experimental interest to consider the temperature range where

$$t_v < \Delta_v \lesssim T \ll t_s < \Delta_s. \quad (1)$$

Upon cooling the system, it is the highest temperature at which one can hope to observe signatures of QSL behaviour. Any precursor diagnostics in this temperature regime would be greatly beneficial before attempting to reach challengingly low temperatures where both quasiparticle species behave quantum coherently ($T < t_v$). In the temperature range given by Eq. (1), visons are thermally populated with a finite density, whereas spinons are sparse and hop coherently across the system on a timescale $O(1/t_s)$ that is fast with respect to the stochastic motion of visons, which occurs on a time scale $O(1/t_v)$ or longer. It is then natural to take a Born–Oppenheimer perspective and treat the visons as static quasiparticles when considering the motion and equilibration of spinons. The slow dynamics of visons allows parallels to be drawn with Falicov–Kimball models [18, 19], and models of quasi-MBL [20–22] and disorder-free localisation [23].

We focus on the case of a \mathbb{Z}_2 topological spin liquid, where there are no direct interactions between spinons and visons that exchange their energy. However, their semionic mutual statistics implies that the spatial arrangement of the visons affects the quantum kinetic energy of the spinons, which in turn

* cc726@cam.ac.uk

mediates an effective, nonlocal interaction amongst the visons. We find that this interplay leads to the localisation of spinons on patches of the system—similar to quantum wells—from which the visons have been expelled in a manner comparable to the Nagaoka effect [24, 25] (see also Ref. [26]).

We provide an effective analytical modelling of these patches that traces their origin to a balancing act between vison configurational entropy and spinon kinetic energy. A remarkable consequence of this behaviour is that the self-localisation of spinons leads to a nonthermal, cooling-rate-dependent density of spinons. This quasiparticle excess likely manifests itself in the spin susceptibility and transport properties of the system as it is cooled from high temperatures. Since this behaviour is inherently related to both the fractionalised nature and the nontrivial mutual statistics of the excitations in the system, it is therefore an important precursor of the QSL behaviour expected at lower temperatures.

Results

Model. We consider for concreteness a toric-code-inspired toy model of a gapped \mathbb{Z}_2 QSL. A possible microscopic derivation of the model is discussed in the Supplementary Note 1, whereas we present here only the essential features of the model in the temperature regime of interest. It can be summarised as a tight-binding model of bosonic spinons with energy cost Δ_s and hopping amplitude t_s on the sites of a square lattice [27]. The visons live on the plaquettes of the lattice, with energy cost Δ_v and occupation numbers $n_p = 0$ or 1. Since the spinons and visons are mutual semions, the latter act as sources of flux of magnitude π , i.e., $\Phi_p = \pi n_p$,

$$H_s(\{n_p\}) = -t_s \sum_{\langle ij \rangle} e^{iA_{ij}} b_i^\dagger b_j + \Delta_s \sum_i b_i^\dagger b_i, \quad (2)$$

where b_i, b_i^\dagger obey the usual hardcore bosonic statistics, $A_{ij} = -A_{ji}$, and $(\nabla \times A)_p = \Phi_p$. Within the Born–Oppenheimer approximation, the spinons remain in their instantaneous eigenstates, with energy $E_s(\{n_p\})$, as different visons configurations $\{n_p\}$ are sampled stochastically, therefore providing an effective energy for the latter. Both spinons and visons are created or annihilated in pairs by virtue of their fractionalised nature.

Generally, one expects spinons in a random π -flux background to be weakly localised (for a recent study, see Ref. 28). At the temperatures considered in this manuscript, the spinons are sparse and the hardcore constraint makes it reasonable on energetic grounds that they will be localised far away from one another. It is therefore sensible in the first instance to investigate the problem of a single isolated spinon. We will later discuss how the results may be extended to the thermodynamic limit with a finite density of spinons.

In order to gain insight into the behaviour of the system, we perform parity-conserving Monte Carlo (MC) simulations of the stochastic ensemble of visons, $\{n_p\}$, on a square lattice containing $L \times L$ sites with periodic boundary conditions, combined with exact diagonalisation of the spinon tight-binding Hamiltonian $H_s(\{n_p\})$ (further details are given in Methods).

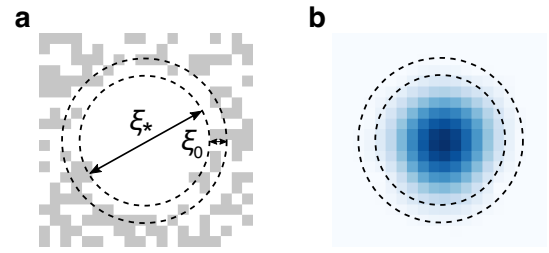


FIG. 1. Equilibrium vison configuration and corresponding spinon ground state density. **a** Vison configuration, $\{n_p\}$. The visons form an empty circular patch surrounded by a disordered background. The inner dashed line corresponds to the saddle point radius ξ_* of the effective free energy (3), while the outer dashed line equals the characteristic extent of the spinon wavefunction, $\xi_* + \xi_0$. **b** Ground state spinon density. The data are taken from the MC simulations at $T/t_s = 10^{-3}$ for a system of size $L^2 = 20^2$ with periodic boundary conditions.

Localisation of spinons. The behaviour of the system is most intuitively illustrated by a snapshot of the vison configuration and of the corresponding spinon ground state probability density in thermodynamic equilibrium at temperature T , as shown in Fig. 1. The spinons are clearly localised in circular patches from which the visons have been totally expelled. We can understand this phenomenon in terms of a competition between the spinon kinetic energy, which favours regions with a low vison density [28], and the vison mixing entropy, which favours a uniform vison density. At finite temperature the balance produces regions of the system from which the visons are expelled, thus providing most of the support for the spinon wave function. In the complementary region, the spinon wave function is exponentially suppressed [29–32] and the visons are in a trivial, noninteracting state.

To confirm this intuition, we propose a toy one-spinon model consisting of an empty circular patch of radius ξ , to which the spinon is confined, while the exterior of the disc is thermally populated with visons, i.e., $p(n_p) \propto e^{-n_p \beta \Delta_v}$. The characteristic free energy $F(\xi)$ of the system as a whole is then given by

$$F(\xi) = \frac{j_0^2 t_s}{(\xi + \xi_0)^2} + \pi T \xi^2 \ln(1 + e^{-\beta \Delta_v}). \quad (3)$$

The first term describes the kinetic energy of the spinon, while the latter corresponds to the entropy of the exterior vison configurations (henceforth, we send $\Delta_v \rightarrow 0$ as it is negligible at the temperatures of interest). The prefactor $j_0^2 t_s$ is set by the ground state energy of an infinite circular well, where j_0 denotes the first zero of the Bessel function $J_0(x)$. The energy gap between the ground state and the first excited state of the quantum well is much larger than the temperature of interest, and thus we assume the spinon to be in the ground state. The phenomenological parameter ξ_0 represents effectively the penetration depth of the spinon wave function into the vison-rich region. We extract ξ_0 numerically by plotting the energy $E(\xi) = j_0^2 t_s (\xi + \xi_0)^{-2}$ as a function of disc radius ξ , averaged over exterior vison configurations (see Methods). There are

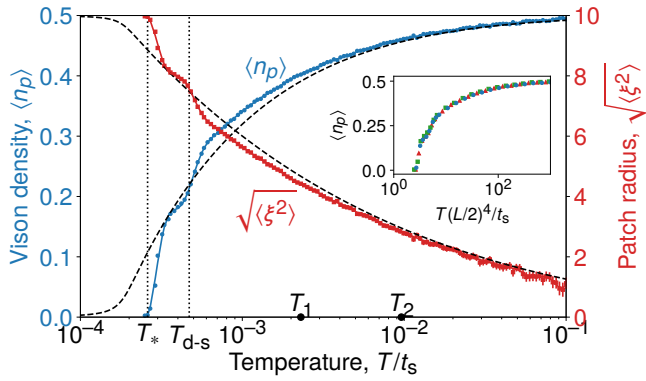


FIG. 2. **Evolution of equilibrium vison density.** We show the average vison density per plaquette, $\langle n_p \rangle$ (blue circles, left vertical scale), and the typical vison-depleted patch radius $\sqrt{\langle \xi^2 \rangle}$ (red squares, right vertical scale) as a function of temperature. The numerical data are compared with the predictions (dashed lines) of the circular disc free energy given in Eq. (3). As temperature is lowered, the finite system makes a transition to a system-spanning strip state (see Supplementary Note 2) at a temperature T_{d-s} , and becomes vison-free below T_* . The solid lines through the MC data are a guide to the eye. The calculations were performed on a system of size $L^2 = 20^2$ satisfying periodic boundary conditions. The inset shows a scaling collapse of $\langle n_p \rangle$ as a function of $T(L/2)^4/t_s$ for $L = 16$ (green squares), 18 (red triangles), 20 (blue circles).

then no adjustable parameters left in the model.

Minimising (3) with respect to ξ yields the typical disc radius $\xi_* \sim T^{-1/4}$ when $\xi_* \gg \xi_0$. To capture thermal fluctuations in the radius ξ , we estimate ξ_* using,

$$\xi_*^2 \equiv \langle \xi^2 \rangle = \frac{1}{Z} \int_0^R d\xi \xi^2 e^{-\beta F(\xi)}, \quad Z = \int_0^R d\xi e^{-\beta F(\xi)}, \quad (4)$$

where R is a cut-off that captures the effect of finite system size in the MC simulations. Other observables may be computed in the same vein.

In Fig. 2 we show the MC data for the average vison density $\langle n_p \rangle$ and the typical patch radius ξ_* for a system of size $L^2 = 20^2$. The vison density is a monotonic function of temperature, and it becomes vanishingly small below a characteristic temperature T_* : As the temperature is lowered, the spinon kinetic energy becomes dominant in the free energy and the vison-depleted patch grows. This behaviour continues until the size of the patch becomes comparable to the size of the system. We find good agreement between the MC simulation and the toy model for $T > T_*$. In our MC simulations on systems of finite size, there exists a competing vison configuration in which, rather than forming a disc, the spinon density (and the corresponding vison-depleted region) forms a strip that wraps around the torus in one direction. Such a configuration typically has a lower vison density and is responsible for the kink observed in the data at the temperature T_{d-s} (see Supplementary Note 2).

The connected correlator $C_\rho(\mathbf{r}_p, \mathbf{r}_{p'}) = \langle n_p n_{p'} \rangle - \langle n_p \rangle \langle n_{p'} \rangle$ is plotted for a range of separations $\mathbf{r}_p - \mathbf{r}_{p'}$ in Fig. 3. The overall agreement between the numerical results and the toy

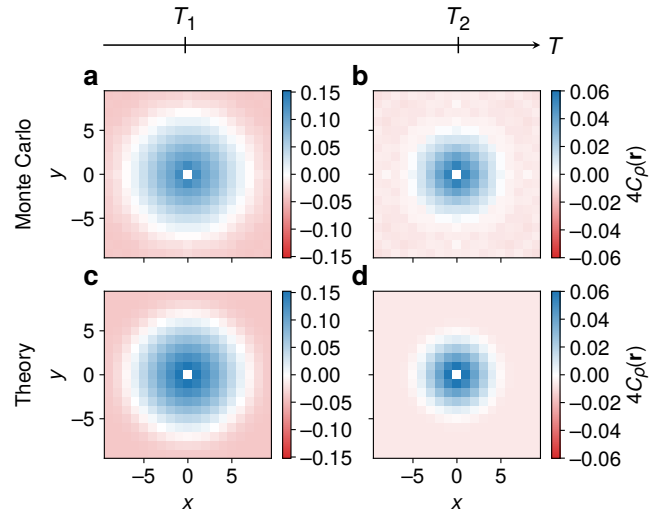


FIG. 3. **Equilibrium real space vison correlations.** Connected vison correlator $C_\rho(\mathbf{r})$, $\mathbf{r} = (x, y)$, at two temperatures (marked for reference also in Fig. 2), **a, c** $T_1/t_s = 2.3 \times 10^{-3}$ and **b, d** $T_2/t_s = 9.6 \times 10^{-3}$. **a, b** correspond to the MC data, while **c, d** are the predictions of the empty disc model. As temperature is increased, the typical size of the vison-depleted patch shrinks and the length scale over which the visons are correlated is correspondingly reduced. The calculations were performed for a system of size $L^2 = 20^2$ satisfying periodic boundary conditions

model over a range of distances and temperatures demonstrates that our intuitive picture is indeed correct. The visons remain correlated over a characteristic distance $2\xi_*$, the typical diameter of the vison-depleted patch, which shrinks with increasing temperature [see Methods for details of the calculations using the disc model, Eq. (4)]. This picture is not modified qualitatively upon addition of weak short-ranged spinon–vison interactions (see Supplementary Note 3).

The toy model (3) predicts that $\xi_* \propto T^{-1/4}$. In a finite system of size L^2 , this means that the vison density vanishes below a critical temperature $T_* \sim t_s L^{-4}$, as we indeed observe in the scaling collapse in the inset of Fig. 2. By contrast, a thermodynamically large system always contains a nonzero density ρ_s of spinons. In this case, since the spinons are effectively hardcore bosons, we expect the visons to form a density ρ_s of independent empty circular patches. This construction applies to the dilute limit where the patch size is significantly smaller than the average distance between spinons, $\xi_* \ll \rho_s^{-1/2}$. Since the thermal spinon density $\rho_s \sim e^{-\beta \Delta_s}$ vanishes exponentially fast as T decreases [33], whereas ξ_* increases only algebraically, the condition is expected to hold in the temperature window of interest (1).

Thermal quenches. The self-localisation of spinons has a number of interesting consequences. Suppose we initialise the system in thermodynamic equilibrium at some finite temperature T_0 , where the condition discussed above, $\xi_* < \rho_s^{-1/2}$, is satisfied. Let us then lower the temperature at a constant rate and follow the evolution of the spinon density ρ_s . The largest

energy scale relevant to spinons is their cost Δ_s , and one therefore expects $\rho_s \sim e^{-\beta\Delta_s}$ if the process is adiabatic. However, the spinons are localised in well-separated patches. To remain in equilibrium as the temperature is lowered, the spinons must annihilate with one another pairwise to reduce their density. They have two annihilation pathways: via tunnelling between two patches—a process which is suppressed in distance due to the localisation of the spinon wave function—or via motion of the patches. The latter process is also slow since it requires a coordinated change in the vison configuration without any energetic driving. Hence, if the cooling rate is sufficiently large, spinon annihilation processes cannot maintain equilibrium and ρ_s develops a plateau.

On the other hand, as the temperature is lowered, the patches continue to grow at a comparatively fast rate, since the process merely requires the (energetically favourable) pairwise annihilation of visons at the edge of each patch. This will progress until the patches eventually come within reach of one another and the spinon annihilation can resume on timescales that are fast compared to the temperature variation. This happens at the threshold $T_* \sim t_s \rho_s^2$. From this time onwards, the spinon density ρ_s resumes its decay; however, it is kinematically locked to the temperature via the relation $T \sim t_s \rho_s^2$. In other words, the spinon density now decreases at an anomalous, out-of-equilibrium rate, $\rho_s \sim \sqrt{T}$. A simple stochastic modelling to illustrate this out-of-equilibrium behaviour is presented in Supplementary Note 5.

Notice that, at this point, if one were to reverse the direction of the temperature variation, upon increasing T the patches shrink and the spinon density ρ_s again remains fixed at a value that is much higher than its equilibrium counterpart. This plateau persists until the temperature T_{th} is reached, where $\rho_s \approx e^{-\Delta_s/T_{\text{th}}}$, at which point the density resumes increasing along the adiabatic curve. One can therefore engineer corresponding hysteretic loops, illustrated schematically in Fig. 4.

We note that the plateaux in ρ_s not only signal a thermodynamic quantity being invariant, but also indicate to a large extent that the positions of the spinons (vison-depleted patches) do not change (their drift motion being a slow process), leading to remarkable memory effects. Any experimental techniques that provide access to the spinon density or its spatial correlators will likely measure signatures of this hysteretic, nonequilibrium behaviour. For instance, the spinon density ρ_s can be directly related to the magnetic susceptibility, $\chi \sim \rho_s$, which can be probed either by thermodynamic measurement or nuclear magnetic resonance through the Knight shift [34, 35]. In thermal equilibrium, ρ_s is exponentially suppressed due to the large spinon gap. However, if the system is cooled rapidly, the aforementioned nonthermal evolution of the spinon density ρ_s manifests itself in an enhancement of χ with respect to the equilibrium value, which may be detected in experiments.

Our results can also be expected to have significant repercussions on transport properties where visons and/or spinons contribute (e.g., thermal transport [36]). The largest effect will likely be from the vison density (and thence their flux), which is reduced by a factor $1 - \pi\rho_s\langle\xi^2\rangle$ due to the spinon patches, and correspondingly acquires a modified temperature dependence. On the other hand, we have already

discussed how the spinon motion is expected to be slow, either via tunnelling from one patch to another area of the system that happens to be sufficiently vison-depleted, or via patch drift. This behaviour is in stark contrast with the regime in which the visons are sparse or absent and spinons can propagate freely throughout the system.

Discussion.

We studied the implications of nontrivial mutual statistics and fractionalisation on excitation densities and their correlations in toric-code-inspired \mathbb{Z}_2 quantum spin liquids at finite temperature. We considered a temperature regime of particular experimental interest in which the low-energy visons are populated thermally, while the energetically costly spinons hop coherently. The balance of spinon kinetic energy and vison configurational entropy leads to the emergence of vison-depleted patches in which the spinons remain localised. Similarly to the way in which ferromagnetic order is favoured by the kinetic energy of a single hole in the Nagaoka effect, here the kinetic energy of a spinon favours vison-free regions in the system. The size of the patches is determined by temperature, with a typical radius that scales as $T^{-1/4}$.

We highlighted important consequences of this phenomenon in the nonequilibrium behaviour of the system in response to temperature ramps. The diffusive motion of the patches is slow, whilst the rate at which they can grow or shrink is energy-driven and hence significantly faster. Since the spinons must annihilate pairwise, this means that the spinon density ρ_s readily falls out of equilibrium upon cooling the system and becomes kinematically locked to $\rho_s \sim \sqrt{T}$. The excess of spinons with respect to their equilibrium density at the same temperature directly affects experimentally relevant quantities such as the magnetic susceptibility and transport properties. Since the effect is inherently due to the combination of nontrivial mutual statistics and fractionalisation of the excitations, its observation would represent an important fingerprint of QSL behaviour. Furthermore, the localisation of spinons on mobile patches would also serve as an indirect signature for the visons, which have hitherto remained elusive in experiments [37].

While the effective model that we discuss, Eq. (2), is derived using perturbation theory (see Supplementary Note 1), we expect that our main conclusions will be applicable outside of this perturbative limit. Indeed, the phenomena that we have described are a direct consequence of (i) the mutual statistics between spinons and visons, and (ii) the separation of energy scales. There is hence a strong reason to believe that these phenomena are robust even when the quantum fluctuations are more appreciable, so long as those prerequisites hold. In particular, spinons and visons remain good quasiparticles as long as the system is not in the immediate vicinity of a confinement/Higgs transition.

So far we have ignored for simplicity any interaction terms between the quasiparticles. While these terms are generally expected, so long as they do not cause the quasiparticles to condense, they only affect the phenomena we discuss quantitatively and not qualitatively. Indeed, interactions between visons would merely alter the form of the classical entropic term in Eq. (3); and short-ranged interactions between spinons

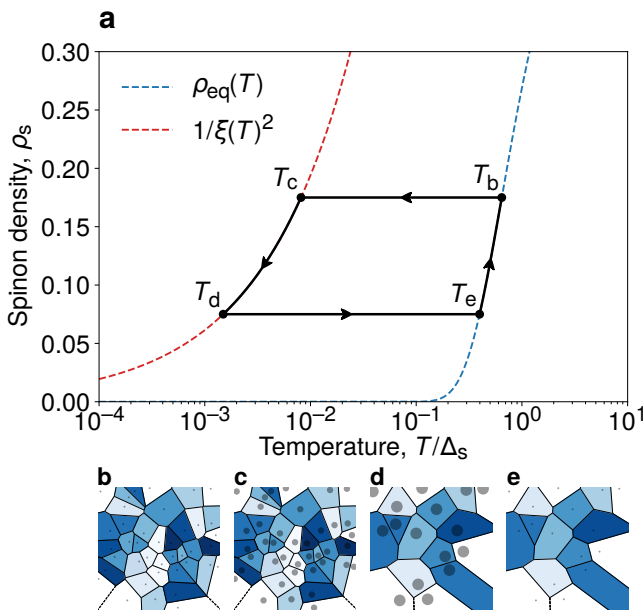


FIG. 4. **Nonequilibrium response of the spinon density to a temperature cycle.** **a** Schematic illustration of the nonequilibrium spinon density. The system is initially prepared in equilibrium at temperature T_b . If temperature is then lowered at a sufficiently large rate, ρ_s falls out of equilibrium—the patches grow in diameter but their diffusive motion is slow. At T_c , the typical separation of the patches becomes comparable to their radius ξ , and the closest pairs begin to annihilate. The density then remains kinematically locked to $1/\xi^2$ as pairs continue to annihilate. If the direction of temperature variation is then reversed at T_d , ρ_s develops another plateau as pairwise annihilation of spinons ceases and the diameter of the patches shrinks. This continues until a sufficiently high temperature, T_e , is reached at which thermodynamic equilibrium is restored. The behaviour of the vison-depleted patches at each of these temperatures is depicted in **b–e**. The patches are qualitatively represented by the solid circles and identified by the colour of their Voronoi cell.

are altogether negligible in the regime where the size of their patches exceeds the characteristic interaction length scale. The only couplings worth investigating in detail are those between spinons and visons, through which the latter can act as diagonal disorder for the former thence also leading to localisation. As we discuss in Supplementary Note 3, in systems satisfying the condition (1), this effect alone is too weak to lead to the formation of well-defined depleted patches.

It is interesting to draw an analogy between the mechanism discussed in our work and the behaviour of type-I superconductors. Indeed, the expulsion of visons from spinon patches operates in a similar manner to the Meissner effect where magnetic vortices are expelled from the superconductor, driven in both cases by a reduction in the quantum kinetic energy of the system [38]. The fact that a very closely related mechanism operates robustly in real materials, leading to experimentally measurable properties, supports the claim that our results are not inherently limited to the theoretical model considered in our work.

We therefore expect our results to apply to gapped \mathbb{Z}_2 spin

liquid candidate materials. For the gapless \mathbb{Z}_2 spin liquids hosted by Kitaev materials, there exists a temperature regime similar to Eq. (1), where the spinons remain quantum coherent whereas the visons are thermally populated. It would be interesting to examine to what extent our results may be generalised to this case.

We note that interference effects also play a role in topological systems with more exotic statistics between the quasiparticles. As shown in Ref. 28, one may generally expect localisation effects, although there are important quantitative differences with respect to the time-reversal-symmetric \mathbb{Z}_2 case. Moreover, if we consider for instance \mathbb{Z}_N theories, the entropy of the exterior vison configuration in Eq. (3) increases, $S \propto \ln N$, favouring a smaller vison-depleted region. All these, as well as the case of non-Abelian statistics, are interesting directions for future work.

Other interesting and open questions include the role of disorder, in particular on transport properties, if it is capable of localising the spinons or pinning the visons in a way that significantly alters the circular shape of the patches. One could also consider how the mechanism generalises to higher-dimensional systems ($d > 2$), both in topological as well as fractonic systems. Mutual statistics is likely to produce similar interference effects; however, dimensionality will play an important role, in particular because topological quasiparticles embedded in higher dimensions usually take the form of extended objects (e.g., closed loops or membranes). Understanding how these quasiparticles may become localised is a challenging and interesting question in its own right [39].

Finally, in our simulations we observed an instability in the shape of the patches at low temperature (from circular to striplike, see Supplementary Note 2). While in our case it is merely a finite size effect due to the spinon wave function overlapping with itself across the periodic boundary conditions, it nonetheless suggests that a similar (possibly nematic) instability may occur in a thermodynamic system when the patches approach one another. Investigating this instability is an interesting future direction, as it affects the spectral properties of the spinons, and possibly alters in a measurable way the response properties of the system.

Methods

Monte Carlo simulations. The thermal average of an observable O that is diagonal in the plaquette operators assumes the form

$$\langle O \rangle = \frac{1}{Z} \sum_{\{n_p\}} \text{Tr} O(\{n_p\}) \exp[-\beta H_s(\{n_p\}) - \beta N_v \Delta_v], \quad (5)$$

where $H_s(\{n_p\})$ is the spinon tight binding Hamiltonian (2), the trace is over the spinon degrees of freedom given a vison configuration $\{n_p\}$, and $N_v = \sum_p n_p$ is the total vison number. $Z = \sum_{\{n_p\}} e^{-\beta N_v \Delta_v} \text{Tr} e^{-\beta H_s(\{n_p\})}$ is the partition function of the system.

Averages of the form (5) can be evaluated efficiently using Markov chain Monte Carlo (MC) applied to the vison degrees of freedom $\{n_p\}$. The proposed updates of the system must however respect the constraint (when imposing periodic

boundary conditions) that the total flux threading the lattice, $\Phi_t = \sum_p \pi n_p$, equals an integer multiple of 2π (equivalently, the total number of vison excitations must be even). Note that the global fluxes threading the torus are chosen to vanish. We make use of the following discrete update, which explicitly preserves the parity of the total number of vison excitations:

- (i) choose two plaquettes p, p' (with $p \neq p'$) at random, and propose the corresponding update to the vison configuration:

$$\begin{aligned} n_p &\rightarrow n'_p \equiv 1 - n_p; \\ n_{p'} &\rightarrow n'_{p'} \equiv 1 - n_{p'}; \end{aligned}$$

- (ii) construct the new spinon tight binding Hamiltonian $H'_s \equiv H_s(\{n'_p\})$ by drawing a string $\gamma_{pp'}$ between the two flipped plaquettes, i.e., setting $A_{ss'} \rightarrow A_{ss'} + \pi$ along the bonds belonging to the path, $\langle ss' \rangle \in \gamma_{pp'}$;
- (iii) diagonalise the new spinon Hamiltonian H'_s to obtain the full energy spectrum;
- (iv) accept the proposed update according to the Metropolis acceptance probability: $\min(1, \text{tr } e^{-\beta H'} / \text{tr } e^{-\beta H})$, where $H = H_s + N_v \Delta_v$.

The initial state of the system is set using a random distribution of visons living on the plaquettes with density $\rho_v = 1/2$ (using even system sizes only, which implies that $\rho_v L^2$ is even, as required). The system is then gradually cooled using $O(10^4)$ MC sweeps, where one MC sweep of the system is equal to $L^2/2$ individual MC steps of the form (i)–(iv). For example, in our simulations of a system of size $L = 20$, decreasing temperatures T_n are taken between $T/t_s = 0.1$ and $T/t_s = 2.5 \cdot 10^{-4}$, in 2^7 logarithmically-spaced increments, with an equilibration time $t_n = \lceil 4 \exp(\alpha/T_n) \rceil$, where α is chosen such that $\sum_n t_n \sim 10^4$. Measurements are then made after this time at each temperature T_n . The parameters in the above cooling protocol are chosen to ensure that the system remains in equilibrium for each measurement. This was checked by calculating the system's characteristic relaxation time, deduced from the decay of the vison autocorrelation function, at several temperatures throughout the cooling protocol (taking care to account for metastability). Finally, the results are averaged over 2^9 independent cooling histories.

In the limit $\beta \Delta_v \ll 1$, the vison energy cost can be safely neglected. We have indeed checked explicitly that adding a small vison chemical potential contribution to the energy of the system does not alter our results quantitatively. Further, one may show using the effective disc free energy that our results are likely to be qualitatively unchanged as long as $\Delta_v \lesssim T_* \sim t_s/L^4$. The vison chemical potential only has an appreciable effect when $T \gtrsim \Delta_v \gtrsim T_*$, in which case, the energetic (rather than entropic) cost of visons becomes substantial, and consequently their density is trivially suppressed.

Spinon ground state energy. The empty disc model assumes that the spinon energy $E(\xi)$, corresponding to a disc of radius

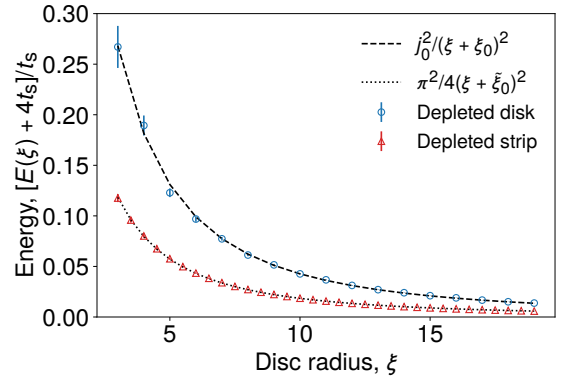


FIG. 5. **Parameterising the spinon ground state energy.** Average ground state energy of a spinon subjected to a vison distribution in which there exists an empty disc of radius ξ (blue circles), or the vison-depleted region forms a strip of width 2ξ that wraps around the torus in one direction (red triangles), surrounded by a disordered region of π -fluxes with average density $1/2$. The dashed and dotted lines correspond to the best fit to functions shown in the legend. The data are averaged over 250 flux realisations in a system of size $L^2 = 40^2$, and the error bars denote the standard deviation of the energy at a given disc radius, not the error in the mean. The parametrisation chosen for $E(\xi)$ on the vertical axis is merely a matter of convenience.

ξ surrounded by disordered visons, can be parametrised as

$$E(\xi) = \frac{j_0^2 t_s}{(\xi + \xi_0)^2}. \quad (6)$$

The numerator $j_0^2 t_s$ is fixed by the large ξ behaviour—in this limit, the energy should be asymptotically described by that of a free particle in an infinite circular well of radius ξ . Hence, j_0 is the first zero of the Bessel function $J_0(x)$. The parameter ξ_0 represents phenomenologically the penetration depth of the spinon wave function into the disordered vison background surrounding the empty circular patch.

In order to fix the value of ξ_0 , we sample random configurations of visons in which there exists an empty disc of radius ξ , and in the complementary region the visons appear randomly with probability $1/2$ per plaquette:

$$p(n_p) = \begin{cases} 0 & \text{if } |\mathbf{r}_p| < \xi, \\ \frac{1}{2} & \text{otherwise.} \end{cases} \quad (7)$$

The resulting ground state energy of the spinon is then averaged over the exterior vison configurations. The resulting averaged energy is plotted in Fig. 5, and a fit to Eq. (6) is performed, leading to the value $\xi_0 = 1.64(2)$. This value does not exhibit significant variation with system size L .

The same method may be applied to the strip vison configuration (discussed further in Supplementary Note 2), also shown in Fig. 5, in which the spinon wave function wraps around the torus in one direction. There are two such configurations in a square system with periodic boundary conditions. The energy

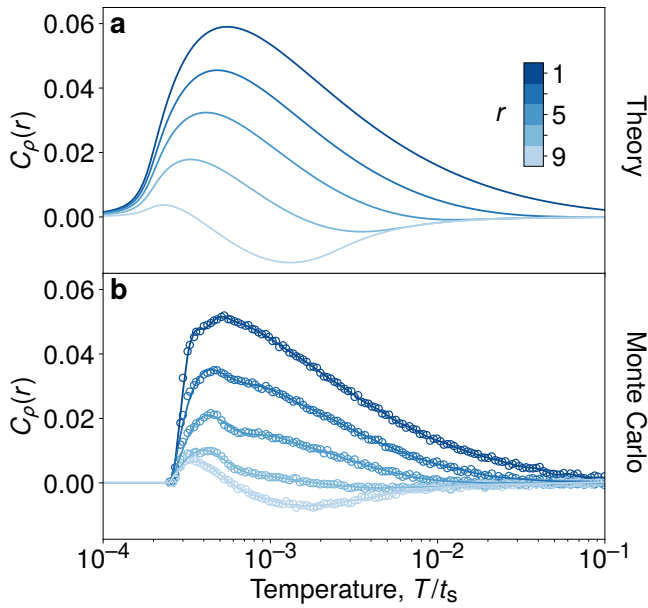


FIG. 6. **Temperature dependence of real-space vison correlations.** We show the vison density correlator $C_\rho(r)$ as a function of temperature at distances $r = 1, 3, \dots, 9$ for a system of size $L^2 = 20^2$. **a** theoretical prediction from Eq. (12) using the disc free energy in Eq. (3). **b** the corresponding MC data. The solid lines through the MC data are a guide to the eye.

of a strip of width 2ξ may be parametrised as

$$E(\xi) = \frac{\pi^2 t_s}{4(\xi + \tilde{\xi}_0)^2}. \quad (8)$$

Fitting the numerical data with this function gives a value $\tilde{\xi}_0 = 1.565(3)$.

Effective empty disc model. The average area $\pi\langle\xi^2\rangle$ of the vison-depleted patch at a given temperature $T = \beta^{-1}$ may be

calculated using the disk free energy in Eq. (3):

$$\langle\xi^2\rangle = \frac{1}{Z} \int_0^R d\xi \xi^2 e^{-\beta F(\xi)}, \quad (9)$$

where $Z = \int_0^R d\xi e^{-\beta F(\xi)}$. Since for temperatures satisfying $T \gg \Delta_v$ the exterior region has a vison density of $1/2$, the average vison density over the system as a whole is

$$\langle n_p \rangle = \frac{1}{2} \left(1 - \frac{\langle\xi^2\rangle}{R^2} \right). \quad (10)$$

Further, since the model assumes that the vison occupation numbers are perfectly correlated within the empty patch, and uncorrelated outside, we may approximate the connected vison correlator in the following way. For two plaquettes separated by the vector \mathbf{r} , with $r = |\mathbf{r}|$, the number of correlated pairs that reside within the disc of radius ξ is given by

$$A(r; \xi) = \Theta(2\xi - r) \left[2\xi^2 \arccos\left(\frac{r}{2\xi}\right) - \frac{r}{2} \sqrt{4\xi^2 - r^2} \right], \quad (11)$$

i.e., the area of intersection of two circles, each with radius ξ , whose centres are separated by a distance r . $\Theta(x)$ is the Heaviside step function. As required, $A(r; \xi)$ vanishes for $r > 2\xi$, and $A(0; \xi) = \pi\xi^2$. The density-density correlator may then be approximated by the cylindrically symmetric function

$$C_\rho(r) \simeq \frac{\langle A(r; \xi) \rangle}{A(r; R)} - \frac{\langle\xi^2\rangle^2}{R^4}. \quad (12)$$

The predictions of Eqs. (10) and (12) are plotted in Figs. 2 and 3, respectively. In Fig. 6 we compare the analytical expression for the correlator $C_\rho(r)$ as a function of temperature, for a range of distances r , with the corresponding MC data.

Data availability

The data that support the findings of this study are available from the corresponding author upon reasonable request.

-
- [1] Chetan Nayak, Steven H. Simon, Ady Stern, Michael Freedman, and Sankar Das Sarma, “Non-abelian anyons and topological quantum computation,” *Rev. Mod. Phys.* **80**, 1083–1159 (2008).
 - [2] Xiao-Gang Wen, “Topological order: From long-range entangled quantum matter to a unified origin of light and electrons,” *ISRN Condensed Matter Physics* **2013**, 198710 (2013).
 - [3] A. Yu. Kitaev, “Fault-tolerant quantum computation by anyons,” *Annals of Physics* **303**, 2–30 (2003).
 - [4] Michael A. Levin and Xiao-Gang Wen, “String-net condensation: A physical mechanism for topological phases,” *Phys. Rev. B* **71**, 045110 (2005).
 - [5] Michael Levin and Xiao-Gang Wen, “Detecting topological order in a ground state wave function,” *Phys. Rev. Lett.* **96**, 110405 (2006).
 - [6] Alexei Kitaev and John Preskill, “Topological entanglement entropy,” *Phys. Rev. Lett.* **96**, 110404 (2006).
 - [7] X. G. Wen and Q. Niu, “Ground-state degeneracy of the fractional quantum hall states in the presence of a random potential and on high-genus riemann surfaces,” *Phys. Rev. B* **41**, 9377–9396 (1990).
 - [8] Frank Wilczek, “New kinds of quantum statistics,” in *The Spin: Poincaré Seminar 2007*, edited by Bertrand Duplantier, Jean-Michel Raimond, and Vincent Rivasseau (Birkhäuser Basel, Basel, 2009) pp. 61–69.
 - [9] Siddharth C. Morampudi, Ari M. Turner, Frank Pollmann, and Frank Wilczek, “Statistics of fractionalized excitations through threshold spectroscopy,” *Phys. Rev. Lett.* **118**, 227201 (2017).
 - [10] Shubhayu Chatterjee, Joaquin F. Rodriguez-Nieva, and Eugene Demler, “Diagnosing phases of magnetic insulators via noise magnetometry with spin qubits,” *Phys. Rev. B* **99**, 104425 (2019).
 - [11] R. B. Laughlin, “Anomalous quantum hall effect: An incompressible quantum fluid with fractionally charged excitations,”

- Phys. Rev. Lett. **50**, 1395–1398 (1983).
- [12] M. Hermanns, I. Kimchi, and J. Knolle, “Physics of the kitaev model: Fractionalization, dynamic correlations, and material connections,” *Annual Review of Condensed Matter Physics* **9**, 17–33 (2018).
- [13] Leon Balents, “Spin liquids in frustrated magnets,” *Nature* **464**, 199–208 (2010).
- [14] Lucile Savary and Leon Balents, “Quantum spin liquids: a review,” *Reports on Progress in Physics* **80**, 016502 (2017).
- [15] J. Knolle and R. Moessner, “A field guide to spin liquids,” *Annual Review of Condensed Matter Physics* **10**, 451–472 (2019).
- [16] L. Balents, M. P. A. Fisher, and S. M. Girvin, “Fractionalization in an easy-axis kagome antiferromagnet,” *Phys. Rev. B* **65**, 224412 (2002).
- [17] Michael Hermele, Matthew P. A. Fisher, and Leon Balents, “Pyrochlore photons: The $U(1)$ spin liquid in a $S = \frac{1}{2}$ three-dimensional frustrated magnet,” *Phys. Rev. B* **69**, 064404 (2004).
- [18] L. M. Falicov and J. C. Kimball, “Simple Model for Semiconductor-Metal Transitions: SmB_6 and Transition-Metal Oxides,” *Phys. Rev. Lett.* **22**, 997–999 (1969).
- [19] Ricardo Ramirez, L. M. Falicov, and J. C. Kimball, “Metal-insulator transitions: A simple theoretical model,” *Phys. Rev. B* **2**, 3383–3393 (1970).
- [20] Mauro Schiulaz, Alessandro Silva, and Markus Müller, “Dynamics in many-body localized quantum systems without disorder,” *Phys. Rev. B* **91**, 184202 (2015).
- [21] N. Y. Yao, C. R. Laumann, J. I. Cirac, M. D. Lukin, and J. E. Moore, “Quasi-many-body localization in translation-invariant systems,” *Phys. Rev. Lett.* **117**, 240601 (2016).
- [22] H. Yarloo, A. Langari, and A. Vaezi, “Anyonic self-induced disorder in a stabilizer code: Quasi many-body localization in a translational invariant model,” *Phys. Rev. B* **97**, 054304 (2018).
- [23] A. Smith, J. Knolle, D. L. Kovrizhin, and R. Moessner, “Disorder-free localization,” *Phys. Rev. Lett.* **118**, 266601 (2017).
- [24] Yosuke Nagaoka, “Ground state of correlated electrons in a narrow almost half-filled s band,” *Solid State Communications* **3**, 409 – 412 (1965).
- [25] Yosuke Nagaoka, “Ferromagnetism in a narrow, almost half-filled s band,” *Phys. Rev.* **147**, 392–405 (1966).
- [26] Márton Kanász-Nagy, Izabella Lovas, Fabian Grusdt, Daniel Greif, Markus Greiner, and Eugene A. Demler, “Quantum correlations at infinite temperature: The dynamical nagaoka effect,” *Phys. Rev. B* **96**, 014303 (2017).
- [27] Julien Vidal, Sébastien Dusuel, and Kai Phillip Schmidt, “Low-energy effective theory of the toric code model in a parallel magnetic field,” *Phys. Rev. B* **79**, 033109 (2009).
- [28] Oliver Hart, Yuan Wan, and Claudio Castelnovo, “Coherent propagation of quasiparticles in topological spin liquids at finite temperature,” *Phys. Rev. B* **101**, 064428 (2020).
- [29] Renate Gade, “Anderson localization for sublattice models,” *Nuclear Physics B* **398**, 499 – 515 (1993).
- [30] Alexander Altland and B D Simons, “Field theory of the random flux model,” *Journal of Physics A: Mathematical and General* **32**, L353 (1999).
- [31] Alexander Altland and B.D. Simons, “Field theory of the random flux model,” *Nuclear Physics B* **562**, 445 – 476 (1999).
- [32] Akira Furusaki, “Anderson localization due to a random magnetic field in two dimensions,” *Phys. Rev. Lett.* **82**, 604–607 (1999).
- [33] O. Hart and C. Castelnovo, “Entanglement negativity and sudden death in the toric code at finite temperature,” *Phys. Rev. B* **97**, 144410 (2018).
- [34] Charles P Slichter, *Principles of magnetic resonance*, Vol. 1 (Springer-Verlag Berlin Heidelberg, 2013).
- [35] Pietro Carretta and Amit Keren, “NMR and μSR in highly frustrated magnets,” in *Introduction to Frustrated Magnetism* (Springer, Berlin, Heidelberg, 2011) pp. 79–105.
- [36] Yoshifumi Tokiwa, Takuya Yamashita, Daiki Terazawa, Kenta Kimura, Yuichi Kasahara, Takafumi Onishi, Yasuyuki Kato, Mario Halim, Philipp Gegenwart, Takasada Shibauchi, Satoru Nakatsuji, Eun-Gook Moon, and Yuji Matsuda, “Discovery of emergent photon and monopoles in a quantum spin liquid,” *Journal of the Physical Society of Japan* **87**, 064702 (2018).
- [37] T. Senthil and Matthew P. A. Fisher, “Fractionalization in the cuprates: Detecting the topological order,” *Phys. Rev. Lett.* **86**, 292–295 (2001).
- [38] L. D. Landau and E. M. Lifschitz, *Electrodynamics of Continuous Media. Course of Theoretical Physics. 8 (2nd ed.)* (Butterworth-Heinemann, 1984).
- [39] Michael Pretko and Rahul M. Nandkishore, “Localization of extended quantum objects,” *Phys. Rev. B* **98**, 134301 (2018).
- [40] <http://www.csd3.cam.ac.uk/>.
- [41] www.dirac.ac.uk.
- [42] Valeriy V. Ginzburg, Leo Radzihovsky, and Noel A. Clark, “Self-consistent model of an annihilation-diffusion reaction with long-range interactions,” *Phys. Rev. E* **55**, 395–402 (1997).
- [43] A.A. Ovchinnikov and V.V. Atrazhev, “The role of space fluctuations in kinetics of recombination of charged particles,” *Physica A: Statistical Mechanics and its Applications* **276**, 1 – 9 (2000).

Acknowledgements

The authors are grateful to Claudio Chamon for several interactions and in particular for suggesting the form of the effective spinon free energy. We would also like to thank Fabian Essler, Austen Lamacraft, Max McGinley, Roderich Moessner and Oleg Tchernyshyov for useful discussions. This work was supported in part by Engineering and Physical Sciences Research Council (EPSRC) Grants No. EP/P034616/1 and No. EP/M007065/1 (C.C. and O.H.), National Natural Science Foundation of China, Grant No. 11974396 and Strategic Priority Research Program of the Chinese Academy of Sciences, Grant No. XDB33020300 (Y.W.). The numerics were performed using resources provided by the Cambridge Service for Data Driven Discovery (CSD3) operated by the University of Cambridge Research Computing Service [40], provided by Dell EMC and Intel using Tier-2 funding from the Engineering and Physical Sciences Research Council (capital grant EP/P020259/1), and DiRAC funding from the Science and Technology Facilities Council [41].

Author contributions

All authors (O.H., Y.W. and C.C.) contributed to the formulation of the study, interpretation of the results and writing of the manuscript. O.H. developed and performed the calculations and numerical simulations.

Competing interests

The authors declare no competing interests.

Supplemental Material for “Correlation holes and slow dynamics induced by fractional statistics in gapped quantum spin liquids”

SUPPLEMENTARY NOTE 1: DERIVATION OF THE MICROSCOPIC MODEL

We focus our attention on a classical \mathbb{Z}_2 lattice gauge theory perturbed by a small, transverse magnetic field h . The model is composed of spin-1/2 degrees of freedom, σ_i , which live on the bonds (labelled by the index i) of a square lattice with $N = L \times L$ sites (labelled by the index s) wrapped around a cylinder

$$H = -J \sum_s A_s - h \sum_i \sigma_i^z, \quad A_s = \prod_{i \in s} \sigma_i^x. \quad (\text{S1})$$

Here $i \in s$ denotes the four spins that reside on the bonds surrounding the lattice site s . The coupling constant J ($\gg h$) is positive by convention. Treating the magnetic field h perturbatively, we arrive at the following ring-exchange Hamiltonian in the ground state sector:

$$H_{\text{eff}}^{(0)} = -J \sum_s A_s - \frac{5}{16} \frac{h^4}{J^3} \sum_p B_p \quad (\text{S2})$$

$$\equiv -\frac{\Delta_s}{2} \sum_s A_s - \frac{\Delta_v}{2} \sum_p B_p, \quad (\text{S3})$$

up to a constant energy shift that arises due to the virtual creation and annihilation of excitations. The plaquette operator B_p is defined as $B_p = \prod_{i \in p} \sigma_i^z$, where $i \in p$ denotes the four spins surrounding the plaquette p . The toric code Hamiltonian [3] is generated perturbatively and lifts the macroscopic degeneracy of the classical \mathbb{Z}_2 theory.

The ground state of the effective model, Supplementary Eq. (S3), is characterised by eigenvalues +1 for all (commuting) operators A_s and B_p (and has a topological degeneracy that is immaterial for the purpose of the present work). Excitations correspond to states in which plaquette operators B_p and/or star operators A_s have negative eigenvalues. We will refer to the energetically costly star defects as spinons, and to the lower-energy plaquette defects as visons ($h^4/J^3 \ll J$, since $J \gg h$ by construction).

Let us then consider the two spinon sector, relevant for the intermediate temperatures of interest, $T \ll h, J$. The magnetic field h makes the spinons dynamical

$$H_{\text{eff}}^{(2)} = 4J - h \sum_{\langle ss' \rangle} \left(b_s^\dagger \sigma_{ss'}^z b_{s'} + \text{h.c.} \right), \quad (\text{S4})$$

where $\langle ss' \rangle$ denotes neighbouring sites on the square lattice, and $\sigma_{ss'}$ is the spin on the bond connecting sites s and s' . Since the magnetic field is applied parallel to the z axis, the vison configuration remains precisely static. The operators b_s, b_s^\dagger are hardcore bosons representing the spinon excitations, which live on the sites of the lattice. Note that the spins $\sigma_{ss'}$ and the operators b_s are not independent: $A_s = e^{i\pi b_s^\dagger b_s}$. Crucially,

each spinon hopping event is accompanied by a spin flip in the σ^x basis. In order to derive an effective tight-binding model, we make a gauge choice by fixing the string, $S(\gamma_i) = \prod_{\langle k\ell \rangle \in \gamma_i} \sigma_{k\ell}^z$, used to define the state corresponding to a spinon residing on site i ; the path γ_i ends on site i . Choosing a different string $S(\tilde{\gamma}_i)$ may lead to an additional phase: $e^{i\phi} = \langle S(\gamma_i) S(\tilde{\gamma}_i) \rangle$, $\phi = 0$ or π . Having made this choice, the hopping matrix element between adjacent sites i, j is given by $t_{ij} = -h \langle S(\gamma_i) S(\gamma_j) \sigma_{ij}^z \rangle$, where $\gamma_i \cup \gamma_j$ and the bond $\langle ij \rangle$ form a closed loop. Moving a spinon around a plaquette p , whose bonds are indexed by $\langle ij \rangle \in p$, the spinon acquires a phase

$$h^{-4} \prod_{\langle ij \rangle \in p} t_{ij} = \left\langle \prod_{\langle ij \rangle \in p} \sigma_{ij}^z \right\rangle = 1 - 2n_p. \quad (\text{S5})$$

The string operators do not appear in Supplementary Eq. (S5) since $S(\gamma_i)^2 = \mathbb{1}$. Hence, for a given vison configuration, and when considering gauge invariant quantities, we can map Supplementary Eq. (S4) onto a nearest neighbour tight-binding model

$$H_{\text{eff}}^{(2)}(\{\phi_{ss'}\}) = 4J - h \sum_{\langle ss' \rangle} \left(b_s^\dagger e^{i\phi_{ss'}} b_{s'} + \text{h.c.} \right) \quad (\text{S6})$$

$$\equiv \Delta_s \sum_s b_s^\dagger b_s - t_s \sum_{\langle ss' \rangle} \left(b_s^\dagger e^{iA_{ss'}} b_{s'} + \text{h.c.} \right), \quad (\text{S7})$$

where the Peierls phases $\phi_{ss'} = -\phi_{s's}$ are, according to Supplementary Eq. (S5), determined by the positions of the visons—each vison contributing a π -flux threading the plaquette on which it resides. With a cylindrical geometry, it is possible to choose a gauge in which the hopping amplitudes are real and uniform in one direction and acquire an appropriate minus sign in the orthogonal direction, according to the specific vison realisation [32]. Imposing periodic boundary conditions, the total flux threading all plaquettes must be an integer multiple of 2π , i.e., $\sum_p (\nabla \times A)_p = 0 \pmod{2\pi}$.

SUPPLEMENTARY NOTE 2: COMPETING STRIP CONFIGURATION

As presented in the main text, the free energy of a spinon confined to a disc of radius ξ surrounded by disordered visons is given by

$$F_d(\xi) = \frac{j_0^2 t_s}{(\xi + \xi_0)^2} + \pi T \xi^2 \ln \left(1 + e^{-\beta \Delta_v} \right). \quad (\text{S8})$$

Neglecting the effects of nonzero ξ_0 , and for temperatures satisfying $T \gg \Delta_v$, one arrives at the following expression for

the radius ξ_* which minimises the disc free energy:

$$\xi_*^d = \left(\frac{j_0^2 t_s}{\pi T \ln 2} \right)^{1/4}. \quad (\text{S9})$$

For $\xi \gg \xi_0$, the disc model then predicts that the system will become completely free of visons at a temperature

$$T_*^d \simeq \frac{16 j_0^2 t_s}{\pi \ln 2 L^4}. \quad (\text{S10})$$

In a square system of finite size with periodic boundary conditions, we observe an instability in our MC simulations whereby the shape of the depleted patch changes upon approaching T_*^d from a disc to a strip wrapping around the system. This is a finite size effect where the spinon wave function overlaps with itself across the periodic boundary conditions. It can be readily understood in light of the competition between the disc free energy and the free energy of a strip of width 2ξ in a system of size $L \times L$, with the corresponding vison strip free energy:

$$F_s(\xi) = \frac{\pi^2 t_s}{4(\xi + \tilde{\xi}_0)^2} + 2T\xi L \ln(1 + e^{-\beta\Delta_v}). \quad (\text{S11})$$

Notice that the strip width that minimises this free energy is, for $\xi \gg \tilde{\xi}_0$ and $T \gg \Delta_v$,

$$\xi_*^s = \left(\frac{\pi^2 t_s}{4TL \ln 2} \right)^{1/3}, \quad (\text{S12})$$

and the temperature at which the system becomes entirely free of visons is given by

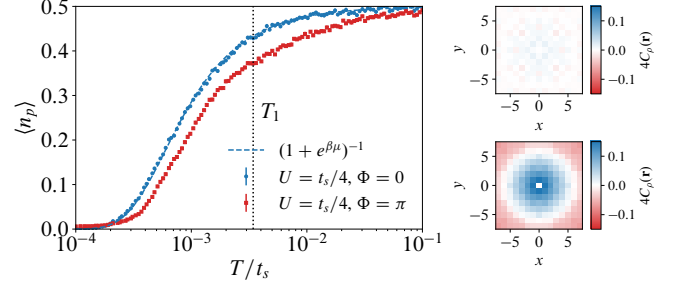
$$T_*^s \simeq \frac{2\pi^2 t_s}{\ln 2 L^4}. \quad (\text{S13})$$

In order to determine whether or not the system makes a transition from the disc state at high temperature to the strip state at low temperature, we compare the two free energies F_d and F_s . Solving for $F_d(T) = F_s(T)$, we find that the two free energies coincide at a temperature

$$T_{ds} = \frac{1}{4} \left(\frac{4}{3} \right)^6 \frac{j_0^6 t_s}{\pi \ln 2 L^4}, \quad (\text{S14})$$

and that the disc free energy is lower than the strip one for $T > T_{ds}$. All of T_*^d , T_*^s , and T_{ds} scale with system size as $\propto L^{-4}$, and therefore the $O(1)$ prefactors determine whether or not an instability between the two vison configurations occurs. We find that $T_*^d, T_*^s < T_{ds}$, which implies that at the level of the saddle point approximation one expects a transition from the disc to the strip state at a temperature given by Supplementary Eq. (S14), before the visons are eventually expelled from the system altogether below T_*^s .

Incidentally, the L^{-4} scaling with system size is indeed confirmed by the numerics in the inset of Fig. 2 in the main text, where the data for the vison density $\langle n_p \rangle$ are shown to collapse for various system sizes L when plotted as a function



Supplementary Figure S1 | Effect of density-density interactions between spinons and visons. Left panel: vison density as a function of temperature in the absence (blue circles) and presence (red squares) of mutual statistics between the spinons and visons. The dashed blue line shows excellent agreement with the density of noninteracting visons in the presence of a uniform chemical potential μ , as discussed in the text. Right panel: corresponding vison correlations at the temperature T_1 indicated by the vertical dotted line on the left panel. In the absence of mutual statistics between the particles, the spinon only endows the visons with an effective chemical potential, but does not induce significant correlations between their positions. The data in both panels are for a system of size $L = 16$, averaged over 2^9 histories.

of TL^4/t_s .

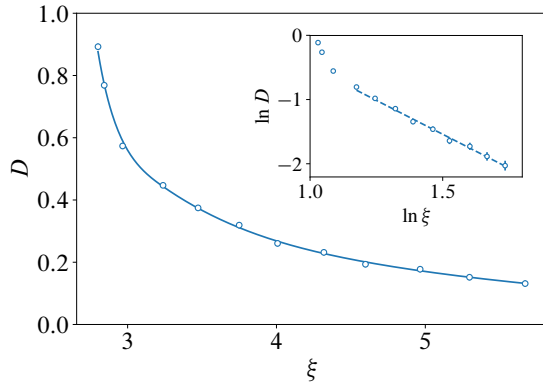
SUPPLEMENTARY NOTE 3: SPINON-VISON INTERACTIONS

Here, we discuss the possibility that the Hamiltonian includes an explicit short-range interaction term between the spinons and visons. In particular, suppose that the spinons and visons are coupled by a density-density term of the form

$$H_{\text{int}} = H_{\text{eff}} + U \sum_s \left(\frac{1}{4} \sum_{p \in s} n_p \right) b_s^\dagger b_s. \quad (\text{S15})$$

That is, each spinon interacts with the four adjacent plaquettes p surrounding each site s (denoted by $p \in s$). The noninteracting Hamiltonian H_{eff} is given by Supplementary Eq. (S7). We expect on rather general grounds that the interactions are repulsive $U > 0$ and weak $|U| < t_s$.

If the mutual statistics between the species is removed, e.g., $A_{ss'} = 0$, then a typical configuration of visons gives rise to a diagonal (on-site) disordered potential term in the spinon tight binding Hamiltonian which also localises the spinons, as is generally expected in two spatial dimensions. However, since interactions are weak ($|U| < t_s$) the localisation length significantly exceeds the lattice spacing and we do not observe the formation of well-defined depleted patches. On the contrary, the vison density behaves smoothly, as if responding to a slowly-varying chemical potential with weak correlations between their positions. This behaviour can be seen in Supplementary Fig. S1, where the strength of the interactions is set to $U = t_s/4$. In these simulations, the localisation length exceeds the system size, and presence of a spinon translates into a uniform chemical potential $\mu \simeq U/L^2$ that controls the vison density as a function



Supplementary Figure S2 | Evolution of the vison-depleted patch diffusion constant with its radius. Dependence of the diffusion constant, D , on the vison-depleted patch radius ξ in equilibrium at temperature T , obtained from MC simulations, where time is measured in units of MC sweeps. The MC data in Fig. 2 of the main text are used to map between temperature and patch radius ξ . The solid line through the MC data is a guide to the eye. The inset shows that $D(\xi)$ is consistent with power law behaviour for sufficiently large ξ : $D \sim \xi^{-2} \sim \sqrt{T}$.

of temperature.

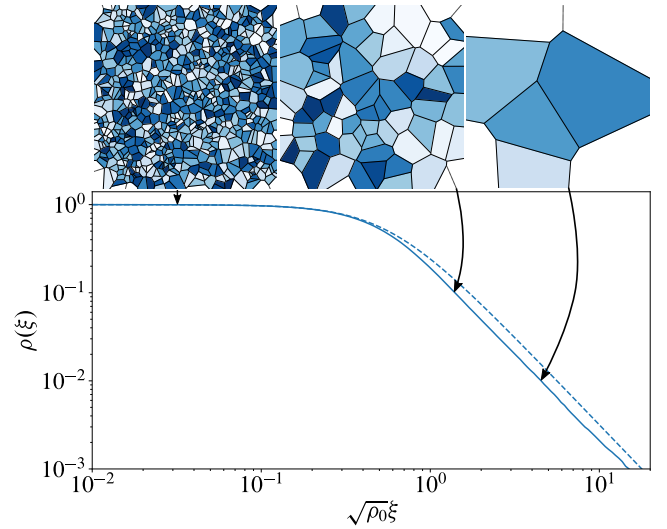
If the mutual statistics between spinons and visons is reinstated, we observe the revival of the nontrivial correlations between the visons, implying the existence of a well-defined vison-depleted patch around the spinon. The linchpin of the formation of the vison-depleted patches and the implied nontrivial vison correlations is an effective disorder that gives rise to a localisation length (i.e., penetration depth) significantly smaller than the radius of the patch $\xi_{\text{loc}} \ll \xi$, which eminently comes about as a result of mutual statistics and not of short-range spinon–vison interactions $|U| < t_s$.

SUPPLEMENTARY NOTE 4: DIFFUSIVE PATCH MOTION

In this section we study the dynamics of the vison-depleted patches as a function of temperature. Since there is no preferred direction for the motion of the patches, one generally expects them to perform an unbiased random walk across the system. Notice however that the motion of a patch over one lattice spacing requires the coordinated rearrangement of a number of visons which scales with the size of the patch. Hence, one expects the diffusion constant, D , (equivalently, the characteristic time scale) of the patch to decrease (grow) with decreasing temperature, as it involves the rearrangement of a larger number of visons.

Let us define the centre of the patch, \mathbf{r}_p , using the maximum of the spinon ground state wavefunction: $|\psi_0(\mathbf{r}_p)|^2 = \max_{\mathbf{r}} |\psi_0(\mathbf{r})|^2$. Asymptotically, one expects that $\langle \mathbf{r}_p^2(t) \rangle \approx 2Dt$. This behaviour is indeed observed in the MC simulations, and the resulting values of D as a function of patch size ξ are shown in Supplementary Fig. S2.

Treating the patches as classical particles that satisfy the reaction-diffusion equation $A + A \rightleftharpoons \emptyset$, one may write down



Supplementary Figure S3 | Evolution of vison-depleted patch density with patch radius. Numerical simulations of the effective patch model: as the radius ξ is increased, all neighbouring pairs of patches separated by a distance 2ξ or less are removed from the system. The centres of the patches remain fixed. The dashed line corresponds to the analytical result in Supplementary Eq. (S18), valid in the dilute limit $\rho \xi^2 \ll 1$, and the solid line corresponds to the numerical results. The data correspond to 25 000 randomly distributed patches, averaged over 20 histories. The Voronoi diagrams show representative configurations of patches at densities ρ_0 , $\rho_0/10$, and $\rho_0/10^2$ (left to right).

an equation for the evolution of the spinon density in the long-wavelength limit [42, 43]

$$\frac{\partial \rho_s}{\partial t} + \nabla \cdot \mathbf{J} = -\mathcal{K} \rho_s^2 + \eta(\mathbf{r}, t), \quad (\text{S16})$$

where the current $\mathbf{J} = -D \nabla \rho_s$, the annihilation constant $\mathcal{K} \propto D$, and $\eta(\mathbf{r}, t)$ is a temperature-dependent source term that represents pairwise creation of the spinons at nonzero temperatures (with appropriate spectral properties). The rate of spinon annihilation in equilibrium is given by $\langle \mathcal{K} \rho_s^2 \rangle$.

In order for the system to fall out of equilibrium as discussed in the main text, the cooling rate must be greater than the rate at which spinons can annihilate in order to remain in equilibrium, i.e., $d\rho_s(T(t))/dt \gtrsim \langle \mathcal{K} \rho_s^2 \rangle$. At the mean field level (i.e., neglecting spatial fluctuations of the spinon density ρ_s), one may estimate the required cooling rate:

$$\left| \frac{dT}{dt} \right| \gtrsim \frac{DT^2}{\Delta_s} e^{-\Delta_s/T}. \quad (\text{S17})$$

Once again we see that, thanks to the exponentially small density of spinons in equilibrium at low temperature, this condition is likely to be easily (if not unavoidably) accessible experimentally in the study of quantum spin liquid materials.

**SUPPLEMENTARY NOTE 5: EFFECTIVE PATCH
GROWTH MODEL**

Here we present an effective model of the growth of randomly distributed vison-depleted patches. The model represents a caricature of the dynamics of the system between temperatures $T_b \rightarrow T_c \rightarrow T_d$ in Fig. 4 in the main text, capturing both the plateau in the density of spinons between $T_b \rightarrow T_c$ and the kinematically-locked regime between $T_c \rightarrow T_d$.

Suppose that the initial density of patches is ρ_0 (equal to the equilibrium spinon density), and that their positions are random and uncorrelated. We assume that the centres of the patches remain stationary, whereas their radii are monodispersed at the typical equilibrium value, ξ , at temperature T . Then, the patches will grow as temperature is reduced until any two patches overlap, at which point the corresponding spinons annihilate. This process is described by the following mean field theory in the dilute limit, $\rho\xi^2 \ll 1$. When changing $\xi \rightarrow \xi + d\xi$ one can infer from geometric arguments that the reduction in the patch density is $d\rho = -8\pi\rho^2\xi d\xi$. One can

then solve for the resulting density

$$\frac{\rho(\xi)}{\rho_0} = \frac{1}{1 + 4\pi\rho_0\xi^2}. \quad (\text{S18})$$

In the limit $\rho_0\xi^2 \ll 1$, the density remains essentially constant and unresponsive. This regime corresponds to the plateau between $T_b \rightarrow T_c$ in Fig. 4. The density begins to decay appreciably once a significant number of the patches start to touch, i.e., $\rho_0\xi^2 \sim 1$. This condition defines the temperature T_c , which represents the crossover between the plateau and the kinematically-locked regime. In the opposite limit, $\rho_0\xi^2 \gg 1$, the density of patches decays as $\rho \sim \xi^{-2}$, corresponding to the kinematically-locked regime between temperatures $T_c \rightarrow T_d$ in Fig. 4. Supplementary Eq. (S18) implies however that $\pi\xi^2\rho = 1/4$ in this regime, which no longer satisfies the condition of diluteness that underpinned our simple modelling. Numerical simulations of the above effective model of patch growth (Supplementary Fig. S3) show that the relationship $\rho \propto \xi^{-2}$ predicted by Supplementary Eq. (S18) does indeed hold in the regime $\rho_0\xi^2 \gg 1$, but with a modified prefactor, $\pi\xi^2\rho \simeq 1/6$.